


Research Article

Nd₂O₃, Cr₂O₃, and V₂O₃ Nanoparticles via Calcination: Synthesis, Characterization, Antimicrobial and Antioxidant Activities

Maged S. Al-Fakeh ^{1,2} and Najla F. Al-Otaibi¹

¹Department of Chemistry, College of Science, Qassim University, Buraidah 51452, Saudi Arabia

²Taiz University, Taiz, Yemen

Correspondence should be addressed to Maged S. Al-Fakeh; alfakehmaged@yahoo.com

Received 31 March 2022; Revised 24 May 2022; Accepted 10 June 2022; Published 6 July 2022

Academic Editor: Brajesh Kumar

Copyright © 2022 Maged S. Al-Fakeh and Najla F. Al-Otaibi. This is an open access article distributed under the Creative Commons Attribution License, which permits unrestricted use, distribution, and reproduction in any medium, provided the original work is properly cited.

Nd₂O₃, Cr₂O₃, and V₂O₃ nanoparticles were prepared by calcining the precursor materials that are novel mixed ligand complexes: [Nd(BDC)(ADMPY)(OAc)].H₂O, [Cr(BDC)(ADM PY)Cl].H₂O, and [V(BDC)(ADMPY)Cl].H₂O, where BDC = 1,4-benzenedicarboxylic acid and ADMPY = 2-amino-4,6-dimethyl pyrimidine. The generated compounds were examined through several techniques such as elemental analysis (C.H.N), UV-Vis spectroscopy, thermal analysis (thermogravimetric, differential thermogravimetry, and differential thermal analysis), FT-IR spectra, X-ray diffraction (XRD), scanning electron microscope (SEM), and transmission electron microscope (TEM). The TEM micrographs showed that neodymium oxide nanoparticles assumed agglomerated platelet-like particles, with particle sizes around 30.16 nm, while chromium oxide NPs showed solid block material with compact density and fewer pores with nearly spherical shape and 56.12 nm size. The vanadium oxide NPs were an agglomeration of small spherical nanoparticles of 28.4 nm size. The antimicrobial properties of the samples were assessed using two strains of Gram-positive bacteria, two strains of Gram-negative bacteria, and one strain of yeast. The antimicrobial results demonstrated that a large spectrum of activity characterizes the tested compounds because they are active on Gram-positive and Gram-negative bacteria, especially on Gram-positive strains. The antioxidant activity of prepared compounds was assessed by scavenging free radicals of DPPH. Metal oxide NPs also showed promising results as antioxidants.

1. Introduction

Antimicrobial resistance is a general health concern because it reduces the efficiency of antimicrobial drugs, which will increase morbidity and mortality as well as health-care costs [1]. Furthermore, free radicals and reactive oxygen species (ROS) are reasoned a several persistent and degenerative illnesses by inflicting oxidative damage to cell molecules [2]. The immoderate generation of ROS in the human physique may additionally result in oxidative stress [3, 4]. Nowadays, searching for novel materials has become critical to overcoming these states. Nanotechnology, since its inception, has had a tremendous impact on the physical, chemical, terrestrial, and biological sciences and has significantly developed recently [5, 6]. This development has made scientists and researchers particularly interested in nanoparticles

because they have a large specific area compared to their size, allowing them to interact with vital elements on the surface of live cells [7]. Metal oxide NPs are one of the most widely used NMs [8]. Compared with organic nanomaterials, metal oxide nanoparticles as inorganic nanomaterials are more applicable because they provide superior hardness, lower toxicity, higher stability, and selectivity [9]. There are various methods for preparing metal oxides, such as the sonochemical method [10–15], sol-gel synthesis [16–18], coprecipitation method [19, 20], solvothermal method [21–23], pyrolysis technique [24, 25], and laser ablation method [26–28]. Calcination has a significant influence on the nanostructure and optical characteristics of nanoparticles. It has the ability to control the size of nanoparticles with a tight size distribution [29]. Calcination also enhances the crystalline, which aids in the removal of impurities from the

samples [30]. Rare earth oxide nanoparticles (Nd_2O_3 NPs) have received a lot of attention as optical and magnetic nanomaterials for various applications because of their distinctive optical properties. All lanthanides share the contractual nature of the protected Nd 4f orbitals, which has a profound impact on their physical properties [31]. It has been used as a catalyst, protective coating, and photonic application [32, 33]. Chromium oxide nanoparticles (Cr_2O_3 NPs) have also received much attention for their value in science and technology. Because chromium has varied stable oxidation states, it can form diverse types of oxides [34]. Particular emphasis has been placed on the composition and properties of chromium oxide (Cr_2O_3) for its importance in specific applications such as green pigment [35], corrosion-resistant [36], and catalysts [37]. Vanadium oxides have been known as energy storage materials in lithium-ion batteries (LIB) due to their structural properties. It exists in varied compositions based on the oxidation states of the vanadium ion [38, 39]. Vanadium trioxide (V_2O_3) has good ionic intercalation properties as well as a high theoretical lithium storage capacity compared to that of V_2O_5 [40]. In addition to its high specific capacity, V_2O_3 has other advantages such as abundant raw material sources and low toxicity [41]. 1,4-benzenedicarboxylic acid and its coordination complexes have great attention in many studies due to their chemical and biological activities [42]. It has bifunctional carboxyl groups and exhibits many coordinate modes; it is common in the preparation of coordination polymers [43, 44]. And it has diverse great features of the compound, which are attributed to their ability to chelate with metal ions [45]. Pyrimidine is the base heterocyclic ring of an essential group of vastly studied materials due to its existence in living systems. Pyrimidines and their derivatives have apparent biological activity and have been used in a variety of fields, from medical to industrial applications [46]. Compared to pyridine bases, the presence of more than one heteroatom in pyrimidine plays an influential role in its coordination chemistry, making it preferable for biological systems [47]. The current paper reports the synthesis of Nd_2O_3 , Cr_2O_3 , and V_2O_3 NPs by calcination of new metal complexes, characterization, and study of their biological activity.

2. Experimental

2.1. Material. The chemicals outlined below were of analytical grade and were used as received were used without being purified further. 1,4-benzenedicarboxylic acid was purchased from Acros, while 2-amino-4,6-dimethyl pyrimidine, neodymium (III) acetate hydrate, chromium (III) chloride hexahydrate, vanadium (III) chloride, and solvents (ethanol, methanol, dimethyl sulfoxide (DMSO), and acetone nitrile) from Sigma-Aldrich.

2.2. Preparation of Metal Complexes

2.2.1. $[\text{Nd}(\text{BDC})(\text{ADMPY})(\text{OAc})].\text{H}_2\text{O}$. This coordination complex was prepared by dissolving neodymium acetate hydrate (4.08 gm) in 15 mL acetone nitrile, then adding it slowly to a solution of BDC (2 gm of H_2BDC in ethanol

20 mL, distilled water 20 mL, and 0.001 M NaOH) with stirring. A methanol/distilled water (10 mL) mixture containing ADMPY (1.48 gm) was added with continued stirring for three days. After being refluxed, the mixture was left to cool to room temperature. Lilac precipitate was filtered, rinsed with distilled water and EtOH, and dried over anhydrous CaCl_2 .

2.2.2. $[\text{Cr}(\text{BDC})(\text{ADMPY})\text{Cl}].\text{H}_2\text{O}$ and $[\text{V}(\text{BDC})(\text{ADMPY})\text{Cl}].\text{H}_2\text{O}$. The mixed ligand complex of 1,4-benzenedicarboxylic acid and 2-amino-4,6-dimethyl pyrimidine with Cr(III) was prepared via dissolving $\text{CrCl}_3 \cdot 6\text{H}_2\text{O}$ (3.20 gm) in 20 mL of distilled water, Then, with stirring, added it dropwise to the BDC solution (2 gm H_2BDC in 20 mL ethanol, 20 mL distilled water, and 0.001 M NaOH). After that, 1.48 gm of ADMPY was dissolved in 15 mL of methanol and 15 mL of water and then added to the mixture with constant stirring for three hours. After reflux, the mixture was left to cool to room temperature. The filtered greenish-blue precipitate was washed with distilled water and ethanol before drying over anhydrous CaCl_2 . For V(III) complex, 1.89 gm of VCl_3 was measured; the same method was followed; and the resulting precipitate was pale brown.

2.3. Preparation of Metal Oxide Nanoparticles. The metal oxide nanoparticles were prepared by direct calcination of Nd(III), Cr(III), and V(III) complexes. The complex powders were placed into a crucible, set in an electric oven, and then calcined at 750°C for three hours, 550°C for two hours, and 600°C for two hours, respectively. The resulting Nd_2O_3 , Cr_2O_3 , and V_2O_3 (light blue, green, and dark gray) nanoparticles (NPs) were washed with EtOH to remove any residual impurities and dried in air, followed by grinding to get fine particles. These were used for different characterizations.

2.4. Characterization of Compounds. Stoichiometric analyses (C.H.N) were performed using a Vario EL elemental analyzer; the physical measurements were measured as reported earlier [48].

2.5. Microbial Strains and Culture Media. In this work, different metal oxide NPs (Nd_2O_3 , Cr_2O_3 , and V_2O_3) in addition to Nd(III) and Cr(III) complexes were tested against Gram-positive and Gram-negative bacterial strains to give insight into their broad-spectrum effect. The used pathogenic strains were two Gram-positive strains “*Staphylococcus aureus* ATCC 25923 (S1) and *Micrococcus luteus* NCIMB 8166 (S4)” and two Gram-negative strains “*Escherichia coli* ATCC 35218 (S5) and *Salmonella typhimurium* ATCC 14028 (S10).” The antifungal activity was evaluated against a pathogenic reference strain of the yeast *Candida albicans* ATCC 90028 (9C). The strains were grown in nutrient broth (Oxoid) at 37°C for 24 hours, and they were cultivated on nutrient agar (Oxoid) at 37°C for 24 hours. The yeast strain was grown in Sabouraud Chloramphenicol broth (Oxoid) at 25°C for 24 hours and cultivated on Sabouraud

Chloramphenicol agar (Oxoid) for 24 h at 37°C. The different strains are listed in Table 1.

2.5.1. Antimicrobial Activity. The antimicrobial activity of the complexes and MONPs was tested using the agar disk diffusion method [49]. Before the test, 50 mg of each extract were dissolved in 1 mL of a solution of dimethylsulphoxide “DMSO” (5%). The strains were cultured for 24 hours at 37°C in Mueller–Hinton (MH) broth (Oxoid), with suspensions adjusted to 0.5 McFarland standard turbidity. After that, 100 μl of each precultured suspension was spread onto MH agar plates. Sterilized filter paper discs (their diameter about 6 mm) were imbibition impregnated with 20 μl of each extract and placed on agar. The treated plates were set at 4°C for 1 hour and then incubated at 37°C for 24 h. After incubation, the diameter of the inhibition zone (clear halo) around the discs was measured. A duplicate of each sample was performed.

2.6. Antioxidant Activity

2.6.1. DPPH Radical Scavenging Assay. According to the method of Mahdhi et al. [50], the free radical scavenging influence of the extracts was evaluated as follows: 1 ml of the sample (5 mg/ml) and 3 ml of a methanol solution of DPPH (2,2-diphenyl-1-picrylhydrazyl) (300 μm) were mixed together. The mixture was vortexed and incubated for 30 min at 25°C. The absorbance of the solution was measured at 517 nm. As a standard, ascorbic acid was employed. The below equation was applied to calculate the DPPH inhibitory ratio:

$$\text{DPPH Scavenging effect (\%)} = \left[1 - \left(\frac{\text{Abs sample}}{\text{Abs control}} \right) \right] \times 100. \quad (1)$$

3. Result and Discussion

The neodymium (III), chromium (III), and vanadium (III) metal complexes were synthesized via the reacting 1,4-benzenedicarboxylic acid and 2-amino-4,6-dimethyl pyrimidine in stoichiometric proportions. These compounds were prepared and used as a starting material for Nd_2O_3 , Cr_2O_3 , and V_2O_3 NPs by the calcination method. The metal complexes are stable in air and insoluble in most organic solvents, while it is partially soluble in dimethylsulphoxide “DMSO.”

3.1. Elemental Analyses (C.H.N). The quantitative elemental analysis for the complexes of the new mixed ligands showed a significant agreement between the experimental and theoretical values of carbon, oxygen, and nitrogen, which confirms the truth of the added ratios of M:L1:L2 (1:1:1), as well as the proposed formulas of these complexes. The results of these analyses are recorded in Table 2.

TABLE 1: The used microbial strains.

Strain	Reference
Gram-positive bacteria	
S1	<i>Staphylococcus aureus</i> ATCC 25923
S4	<i>Micrococcus luteus</i> NCIMB 8166
Gram-negative bacteria	
S5	<i>Escherichia coli</i> ATCC 35218
S10	<i>Salmonella typhimurium</i> ATCC 14028
Yeast	
9C	<i>Candida albicans</i> ATCC 90028

3.2. Molar Conductivity Measurement. The molar conductivity of the coordination compounds was measured at room temperature in dimethylsulphoxide using 10^{-3}M solutions of complexes; the results showed that all compounds had low conductivity values that were evidence that they were nonionic (Table 2).

3.3. Infrared Spectra. The most salient feature in the IR spectra of Nd(III), Cr(III), and V(III) complexes (Table 3) was the existence of two strong bands in the 1,556–1,558 and 1,374–1,394 cm^{-1} region, referred to the asym (COO) and sym (COO) stretching vibrations of the BDC ligand [45]. The absence of the characteristic band of carboxylic acids at 1,715–1,680 cm^{-1} indicates the complete deprotonation of the dicarboxylic acid molecule [51]. The separation value of $\Delta\nu \leq 192 \text{ cm}^{-1}$ indicates a bidentate form of coordination for the carboxylate group [45]. The $\delta(\text{O-C-O})$ in-plane appears vibration at 728–748 cm^{-1} [52]. Furthermore, the frequencies of asym (NH_2), sym (NH_2), (NH_2), and C- NH_2 occurring in free ADMPY at 3,312, 3,391, 1,628, and 1,250 cm^{-1} , respectively, were found to have no shift in all complexes; this indicates that the amino group does not participate in the bonding [53, 54]. The $\nu(\text{C=N})$ spectra appear as two bands at 1,574–1,577 and 1,648–1,653 cm^{-1} compared to the free bond (1,570 cm^{-1}); these changes indicate the unequal mode of the N-atoms of the heterogeneous cycle in the compound, which indicates that the coordination mode is monodentate [53, 55]. Also, $\nu(\text{C=C})$ and $\nu(\text{C-N})$ bands appear at 1,476–1,478 cm^{-1} and 1,317–1,320 cm^{-1} , respectively [53]. These results are consistent with the coordination of ADMPY through the heterocycle nitrogen atom in complexes. The stretching vibration of $\nu(\text{CH}_3)$ for all complexes appeared at 2,985–2,989 cm^{-1} [53]. The spectra of complexes also showed bands in the 3,438–3,447 and 505–510 cm^{-1} range, which is attributed to νOH in lattice and wagging water, respectively [52]. The spectrum of neodymium (III) complex appears as bands at 1,568 and 1,339 cm^{-1} , which are assigned to the acetate group, with separation value $\Delta\nu = 229 \text{ cm}^{-1}$, indicating monodentate mode [56]. Additionally, Cr(III) and V(III) complexes show bands at 418 and 420 cm^{-1} corresponding to metal chloride [57]. M-oxygen and M-nitrogen bonding appear in spectra at 552–570 and 469–472 cm^{-1} regions, respectively [58]. FT-IR spectra of metal complexes are shown in Figure 1.

TABLE 2: Color, elemental analysis, and decomposition point of the mixed ligand complexes.

Complexes	M.F. (M.Wt.)	Color	Found (calcd. %)			m.p. (°C decomp.)	Λ_m (Scm ² mol ⁻¹)
			C	H	N		
[Nd(BDC)(ADMPY)(OAc)].H ₂ O 1	C ₁₆ H ₁₈ N ₃ NdO ₇ (508.58)	Lilac	38.06 (37.78)	4.17 (3.56)	8.89 (8.26)	<300	32.5
[Cr(BDC)(ADMPY)Cl].H ₂ O 2	C ₁₄ H ₁₅ N ₃ ClCrO ₅ (392.74)	Greenish- blue	42.96 (42.81)	3.97 (3.84)	10.90 (10.69)	253	23.1
[V(BDC)(ADMPY)Cl].H ₂ O 3	C ₁₄ H ₁₅ N ₃ ClVO ₅ (391.69)	Pale brown	43.60 (42.92)	4.05 (3.86)	11.09 (10.72)	260	37.1

1, 2, and 3 are the numbers of three compounds.

TABLE 3: FT-IR spectral data of ligands and their metal complexes.

Group	BDC	ADMPY	Nd (III)	Cr (III)	V(III)
COOH	1,715–1,680	—	—	—	—
ν (COO) asym.	—	—	1,556	1,557	1,558
ν (COO) sym.	—	—	1,394	1,376	1,374
ΔV	—	—	162	181	184
C=N	—	1,570	1,576	1,577	1,574
H ₂ O lattice	—	—	3,440	3,447	3,438
ρw (H ₂ O)	—	—	505	508	510
OAc	—	—	—	—	—
ν (COO) asym	—	—	1,568	—	—
ν (COO) sym.	—	—	1,339	—	—
ΔV	—	—	229	—	—
M-O	—	—	552	570	567
M-N	—	—	472	470	469
M-Cl	—	—	—	418	420

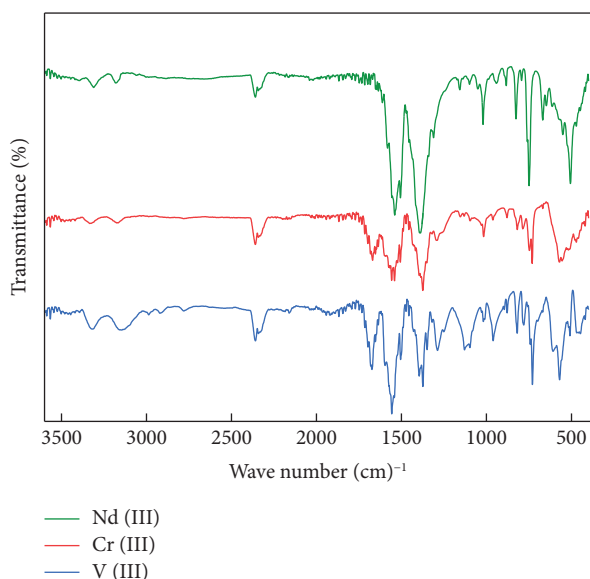


FIGURE 1: IR spectrum of Nd(III), Cr(III), and V(III) compounds.

3.4. Electron Spectra. Electronic spectra of metal complexes and MONPs were recorded using DMSO as solvent (Table 4). The spectra showed two characteristic bands in the ranges of 33,445–34,014 and 40,000–40,816 cm⁻¹, assignable to $\pi \rightarrow \pi^*$ and $n \rightarrow \pi^*$ transitions within the BDC and ADMPY [46, 59, 60]. Furthermore, the f-f transition was found in the spectrum of the Nd(III) complex due to the transitions within 4f levels, which are usually forbidden but

may become allowed after 5s² 5p⁶ electrons remove the degeneracy of 4f orbitals. The transition at 17,575 cm⁻¹ corresponds to transition from the ⁴I_{9/2} → ⁴G_{5/2} suggesting their octahedral structure [61]. Also, there are distinct bands attributed to the d-d transitions of the chromium (III) and vanadium (III) complexes. For spectra of Cr(III) complex, three bands at 26,525, 20,450, and 18,248 cm⁻¹ attributed to the ⁴A_{2g} → ⁴T_{1g} (P), ⁴A_{2g} → ⁴T_{1g} (F), and ⁴A_{2g} → ⁴T_{2g} (F) transitions, respectively, in agreement with octahedral geometry [62], while V(III) complex observe two bands at 19,268 and 14,728 assignable to the ³T_{1g} → ³T_{1g} (P) and ³T_{1g} → ³T_{2g} (F), respectively, indicating their octahedral geometry [63]. On the other hand, the spectra in Figures 2–4 showed a characteristic absorption peak for metal oxide nanoparticles, which was matching with the literature. The spectrum appears as bands at 247, 391, and 246 nm attributed to Nd₂O₃, Cr₂O₃, and V₂O₃, respectively [64–66].

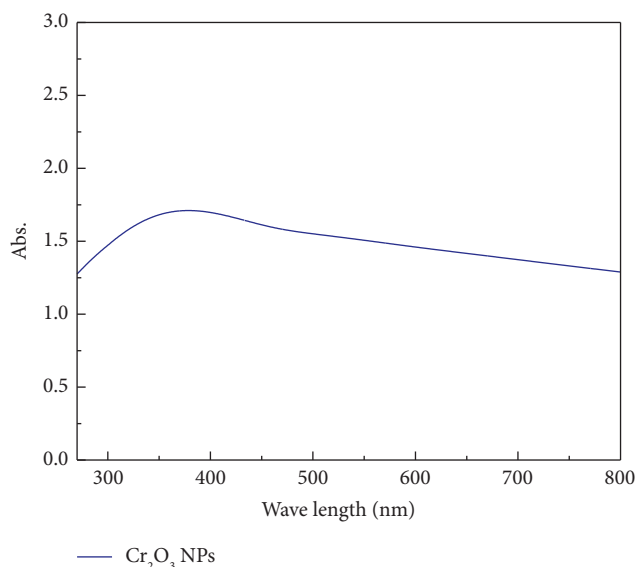
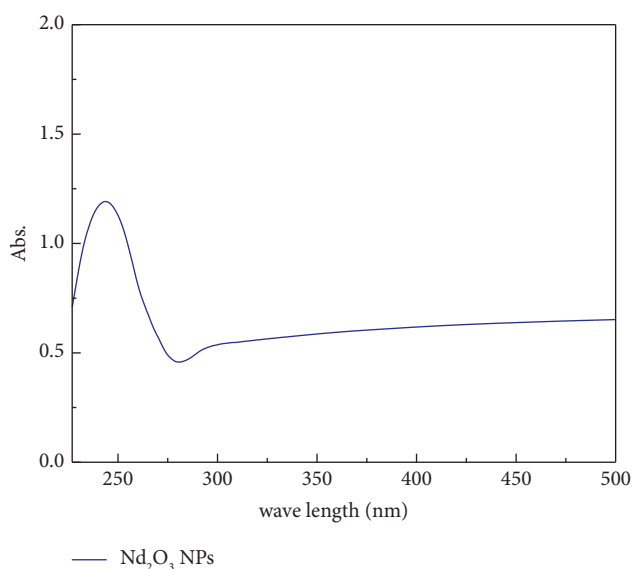
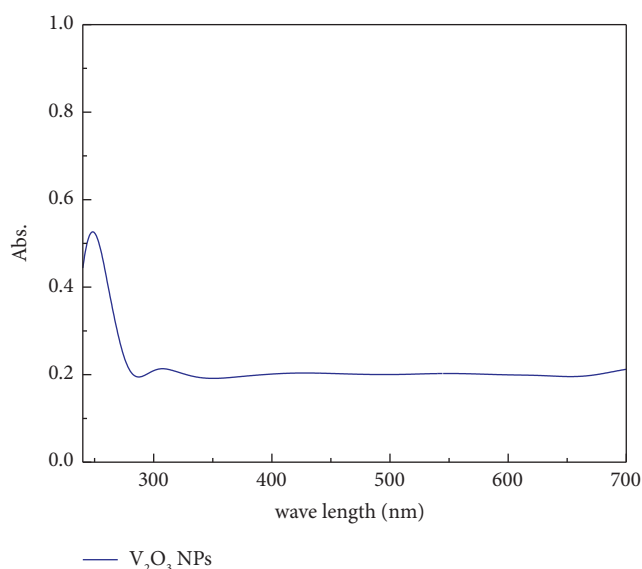
3.5. Magnetic Moment. The measurements of magnetic susceptibility in the solid-state display that the metal complexes are paramagnetic at 25°C. The magnetic moment of the Nd(III) complex was 3.70 B.M. [67], while the Cr(III) complex was 3.56 B.M. [68]. And the V(III) complex was 2.54 B.M. [69], all of which were in agreement with the values reported for octahedral complexes (Table 4; Figures 5–8).

3.6. Thermal Analysis. The thermal data of complexes were listed in Table 5, and the steps were represented in Scheme 1.

3.6.1. [Nd(BDC)(ADMPY)(OAc)].H₂O. The Nd(III) complex undergoes a stepwise decomposition in four steps of weight losses in the temperature ranges 51–140°C, 142–200°C, 202–303°C, and 305–550°C (Figure 9 and Scheme 1). The first observed mass loss was attributed to a lattice water molecule (calc. 3.54%, found 3.10%). The DTG peak occurs at 105°C, and an exothermic peak arises at 107°C in DTA. The second step indicates the release of acetate (calc. 11.60%, found 10.76%). The DTG curve exhibits this stage at 147°C and the related DTA exothermic peak at 149°C. The observed mass loss of the third step agrees with the loss of the ADMPY decomposition (calc. 24.21%, found 24.68%; DTG midpoint at 247°C). For this step, the DTA curve displays a broad exothermic peak at 249°C. The fourth step reveals the decomposition of the BDC molecule (calc.

TABLE 4: Absorption spectra and magnetic moment of metal complexes.

Compound	λ max. (nm)	λ max. (cm^{-1})	Assignment	μ_{eff} (B.M.)
BDC	240	41,667	$\pi \rightarrow \pi^*$	—
ADMPY	290	34,483	$n \rightarrow \pi^*$	—
Nd(III)	254	40,000	$\pi \rightarrow \pi^*$	3.70
	295	33,898	$n \rightarrow \pi^*$	
	569	17,575	${}^4I_{9/2} \rightarrow {}^4G_{5/2}$	
Cr(III)	245	40,816	$\pi \rightarrow \pi^*$	3.56
	299	33,445	$n \rightarrow \pi^*$	
	377	26,525	${}^4A_{2g} \rightarrow {}^4T_{1g}$ (P)	
	489	20,450	${}^4A_{2g} \rightarrow {}^4T_{1g}$ (F)	
	548	18,248	${}^4A_{2g} \rightarrow {}^4T_{2g}$ (F)	
V(III)	249	40,161	$\pi \rightarrow \pi^*$	2.54
	294	34,014	$n \rightarrow \pi^*$	
	679	14,728	${}^3T_{1g} \rightarrow {}^3T_{2g}$ (F)	
	519	19,268	${}^3T_{1g} \rightarrow {}^3T_{1g}$ (P)	

FIGURE 3: UV-Vis spectrum of Cr_2O_3 NPs.FIGURE 2: UV-Vis spectrum of Nd_2O_3 NPs.FIGURE 4: UV-Vis spectrum of V_2O_3 NPs.

32.27%, found 28.76%), with a corresponding DTG peak at 410°C and a broad exothermic peak at 413°C in DTA. The final product is assigned to 1/2 neodymium (III) oxide (calc. 33.08%, found 32.70%).

3.6.2. $[\text{Cr}(\text{BDC})(\text{ADMPY})\text{Cl}]\cdot\text{H}_2\text{O}$. For the thermal behavior of the Cr(III) complex, the thermogram indicates four distinct mass loss stages at $54\text{--}122^\circ\text{C}$, $124\text{--}212^\circ\text{C}$, $214\text{--}382^\circ\text{C}$, and $384\text{--}550^\circ\text{C}$. The first step is consistent with the release of the lattice water molecule (calc. 4.58%, found 3.66%). The DTG peak at 100°C corresponds to an exothermic peak in the DTA curve at 103°C . The second step shows a mass loss corresponding to chloride anion (calc. 9.02%, found 8.10%), with a DTG midpoint at 155°C associated with an

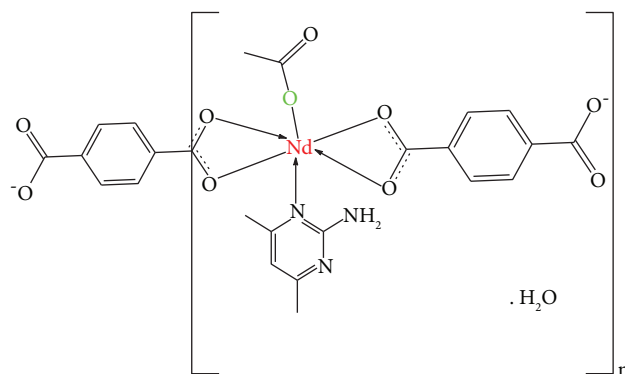


FIGURE 5: Suggesting structure of Nd(III) coordination polymer.

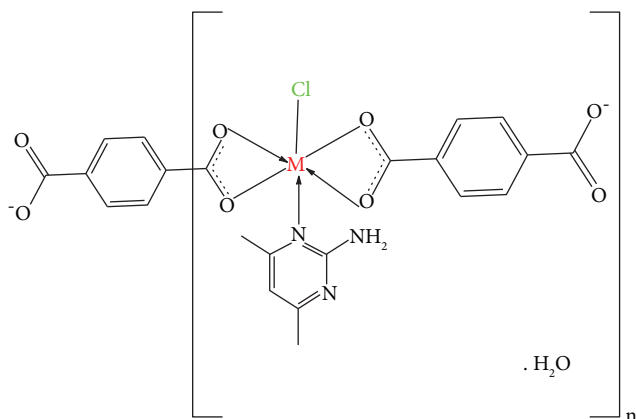


FIGURE 6: Suggesting structure of Cr(III) and V(III) coordination polymers ($M = \text{Cr}$ or V).

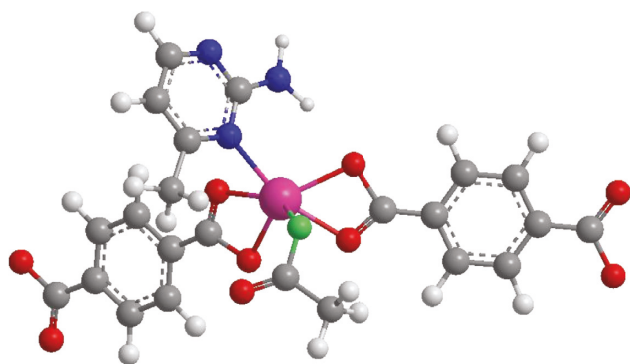


FIGURE 7: Coordination geometry (Nd) atom. Pink: Nd, red: O, blue: N, and green: OAc.

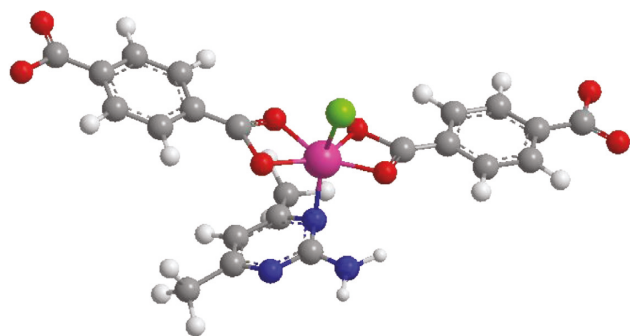


FIGURE 8: Coordination geometry around (Cr or V) atom. Pink: Cr or V, red: O, blue: N, and green: Cl.

exothermic peak at 157°C . The third and fourth stages relate to the release of ADMPY and BDC (calc. 73.14%, found 69.32%). Related DTG peaks at 379 and 400°C were merged in the DTA curve into one broad step centered at around 403°C . The final product is $1/2 \text{Cr}_2\text{O}_3$ (calc. 19.34%, found 18.92%).

3.6.3. $[\text{V}(\text{BDC})(\text{ADMPY})\text{Cl}]\cdot\text{H}_2\text{O}$. For V(III) complex, the TG curve is characterized by four decomposition steps at four steps. These steps occur in the temperature ranges

$40\text{--}128^{\circ}\text{C}$, $130\text{--}226^{\circ}\text{C}$, $228\text{--}329^{\circ}\text{C}$, and $331\text{--}550^{\circ}\text{C}$. Elimination of the lattice water molecule (calc. 4.60%, found 4.12%) was observed at the first step. This step is related to a DTG peak at 77°C with an exothermic at 79°C in the DTA curve. The second step indicates the released chlorine ion (calc. 9.05%, found 8.76%). The corresponding DTG peak was seen at 198°C , with an exothermic peak at 200°C in the DTA curve. The third mass loss is compatible with the decomposition of the ADMPY ligand (calc. 31.44%, found 30.55%). The DTG curve shows this stage as a rise at 298°C , related to an exothermic peak at 301°C in the DTA curve. The fourth step corresponds to BDC decomposition (calc. 41.90%, found 36.74%). DTG peak at 405°C is associated with a broad exothermic peak in the DTA curve at 407°C . The residual part agrees with the formation of $1/2 \text{V}_2\text{O}_3$ (calc. 19.13%, found 20.83%).

3.7. XRD Study. The XRD pattern of the synthesized Nd(III), Cr(III), and V(III) complexes is shown in Figures 10–12, while Figures 13–15 show the XRD pattern of Nd_2O_3 , Cr_2O_3 , and V_2O_3 NPs on the scale of $2\theta = 10\text{--}80$. The sharp, strong peaks prove the products were well crystallized, while the broadening in the patterns indicates that the particles are of nanoscale [70]. The average particle size of the synthesized compounds was calculated by Scherrer's equation. Crystal structure data for complexes and MONPs are listed in Tables 6 and 7.

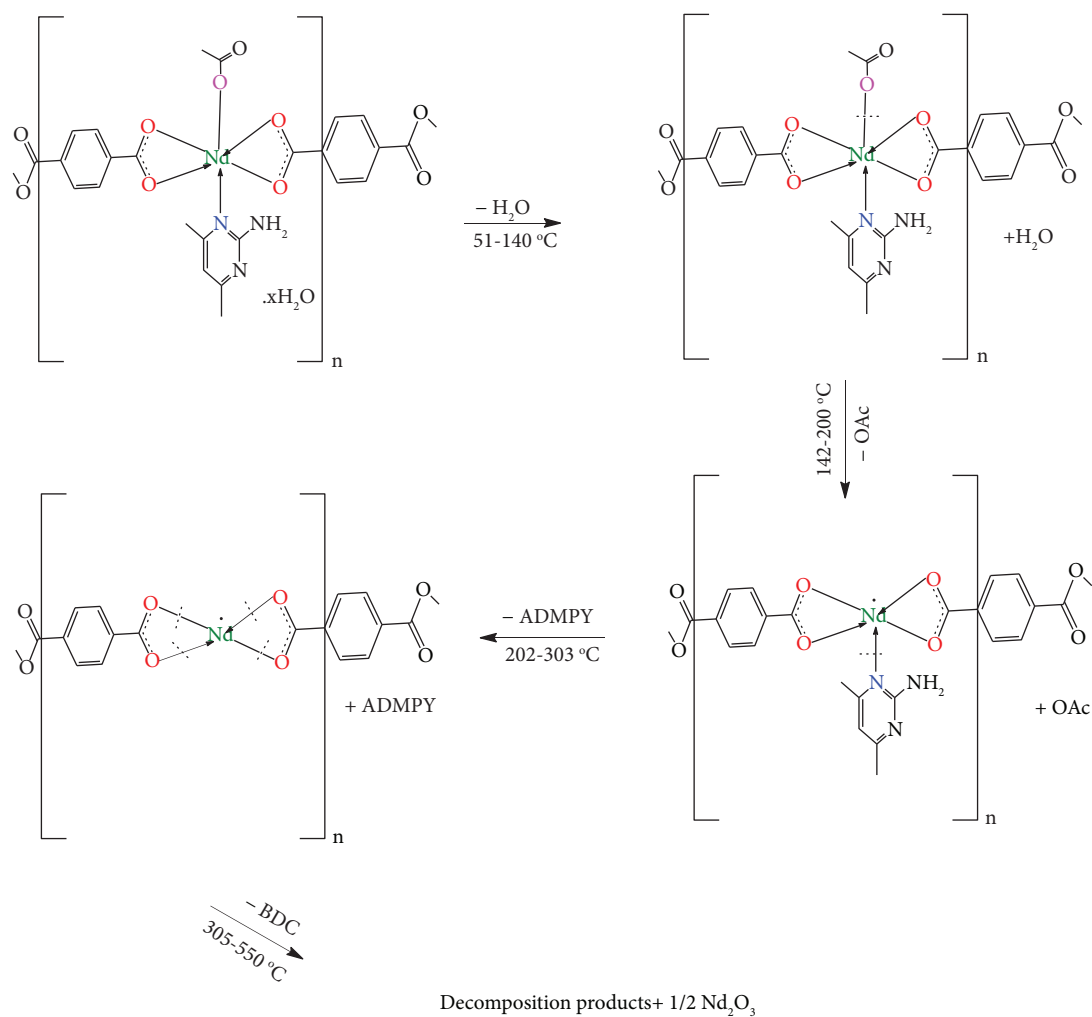
3.8. Electron Microscope (SEM and TEM). Changes in the size and morphology of the nano-metal oxides during the synthesis process were assessed using SEM. The morphologies of three MONPs are shown in Figures 16–18. Nd_2O_3 NPs clearly show agglomerated platelet-like particles, with particle size around 30.16 nm , while Cr_2O_3 NPs show solid block material with compact density and fewer pores with nearly spherical shape and 56.12 nm size. The V_2O_3 NPs were an agglomeration of small spherical nanoparticles in 28.4 nm size. On the other hand, TEM images (Figures 19–21) coincided nicely with the SEM images. Nd_2O_3 displayed a heterogeneous structure with an aggregation of particles, with more platelet-like particles of about 26.9 nm . As for the Cr_2O_3 NPs, some dispersed nanoparticles can be seen clearly in the TEM image with a subspherical shape with a diameter of 53.2 nm . Spherical shapes and agglomeration of particles can be seen clearly in the V_2O_3 NPs image, with a size of 21.32 nm . These results are well in agreement with the XRD analysis.

3.9. Antimicrobial and Antioxidant Assays. The antimicrobial results summarized in Table 8 and Figures 22–25 demonstrate that a large spectrum of activity characterizes the tested compounds because they are active on Gram-positive and Gram-negative bacteria, especially on Gram-positive strains. Except for metal oxide nanoparticles, other compounds are characterized by a variable activity depending on the strain with the zone of inhibition, which varies between 1 and 2 cm. As summarized in Table 8, the

TABLE 5: Thermal analysis of metal compounds.

Compounds	TG range (°C)	DTG (°C)	Mass loss (%)		Assignment
			Calc. (%)	Found (%)	
[Nd(BDC)(ADMPY)(OAc)].H ₂ O 1	51–140	105	3.54	3.10	Loss of hydrated water
	142–200	147	11.60	10.76	Loss of acetate group
	202–303	247	24.21	24.68	Loss of ADMPY
	305–550	410	32.27	28.76	Loss of BDC
	—	—	33.08	32.70	The residue (1/2 Nd ₂ O ₃)
[Cr(BDC)(ADMPY)Cl]. H ₂ O 2	54–120	100	4.58	3.66	Loss of 2 H ₂ O
	122–212	155	9.02	8.10	Loss of chloride ion
	214–382	379	73.14	69.32	Loss of organic ligands
	384–550	400	—	—	—
	—	—	19.34	18.92	The residue (1/2 Cr ₂ O ₃)
[V(BDC)(ADMPY)Cl]. H ₂ O 3	40–128	77	4.60	4.12	Loss of hydrated water
	130–226	198	9.05	8.76	Loss of chloride ion
	228–329	298	31.44	30.55	Loss of ADMPY
	331–550	405	41.90	36.74	Loss of BDC
	—	—	19.13	20.83	The residue (1/2 V ₂ O ₃)

1, 2, and 3 are the numbers of three compounds.



SCHEME 1: Decomposition of Nd(III) compound in dynamic air.

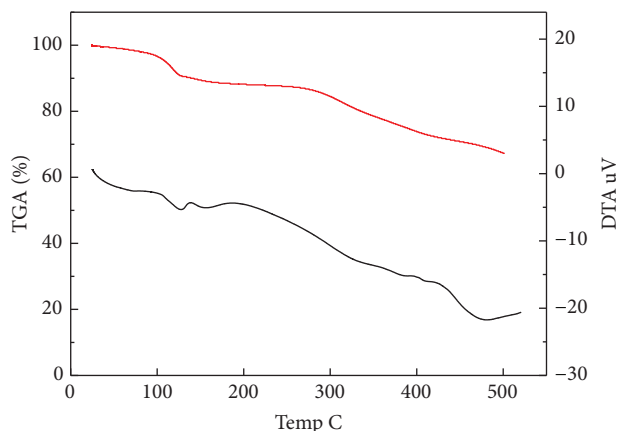
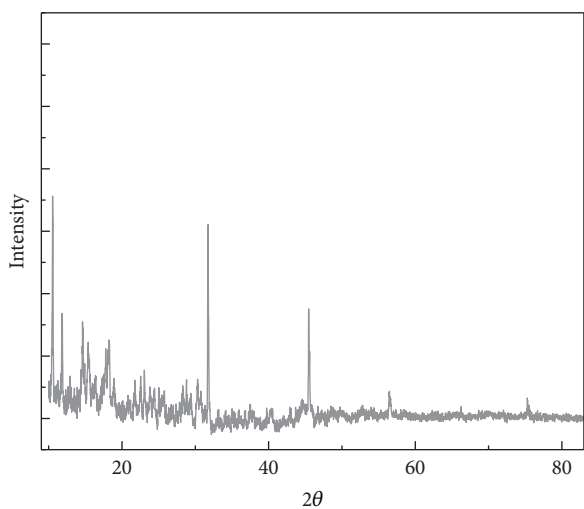
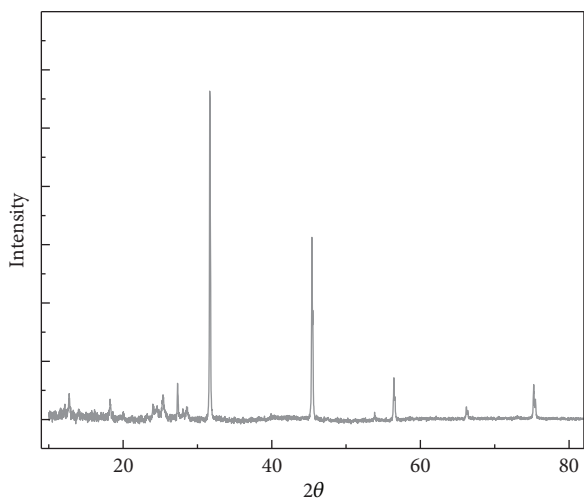


FIGURE 9: TGA and DTA thermograms of Nd(III) compound.



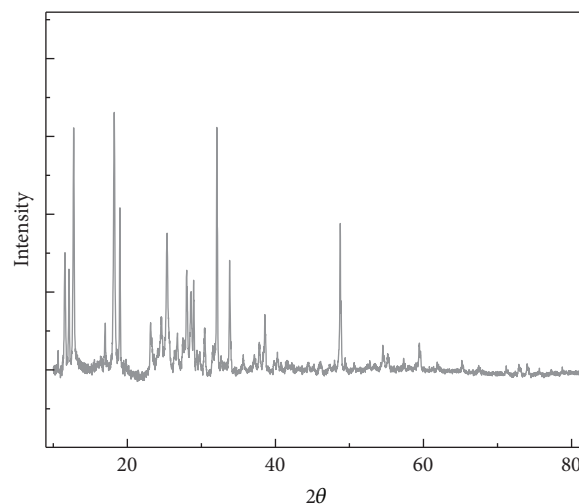
— Nd (III) Complex

FIGURE 10: XRD pattern of Nd(III) compound.



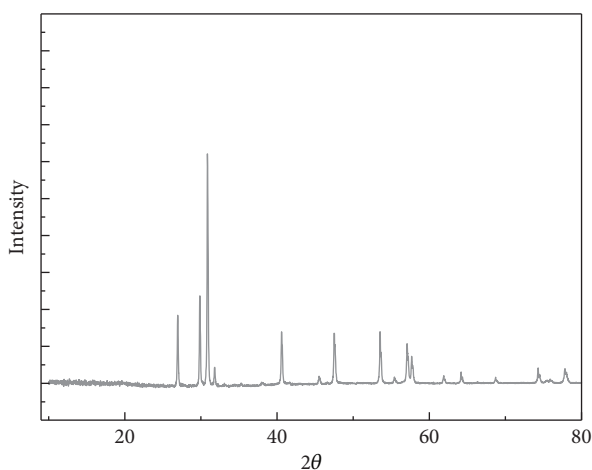
— Cr (III) Complex

FIGURE 11: XRD pattern of Cr(III) compound.



— V (III) Complex

FIGURE 12: XRD pattern of V(III) compound.



— Nd₂O₃ NPs

FIGURE 13: XRD pattern of Nd₂O₃ NPs.

results demonstrated a promising antioxidant activity for Nd₂O₃, Cr₂O₃, and V₂O₃ nanoparticles with a DPPH scavenging percentage ranging between 6.0 and 52%. The evaluated extracts also revealed an antifungal activity against *Candida albicans* except for Cr(III) complex, which is still inactive.

The data in Table 8 showed that the Nd₂O₃, Cr₂O₃, and V₂O₃ nanoparticles displayed perfect activity against bacterial and fungal strains. The Gram-positive bacteria cell consists of a thick wall; it is a peptidoglycan molecule. Since peptidoglycans are molecules that have a negative charge, they link positive ions emitted from metal oxide NPs in the liquid growth medium. Gram-negative bacteria such as *E. coli* may allow more positive ions to penetrate the plasma membrane, but they are typically less resistant to antibiotics and antibacterial treatments than Gram-positive bacteria [71].

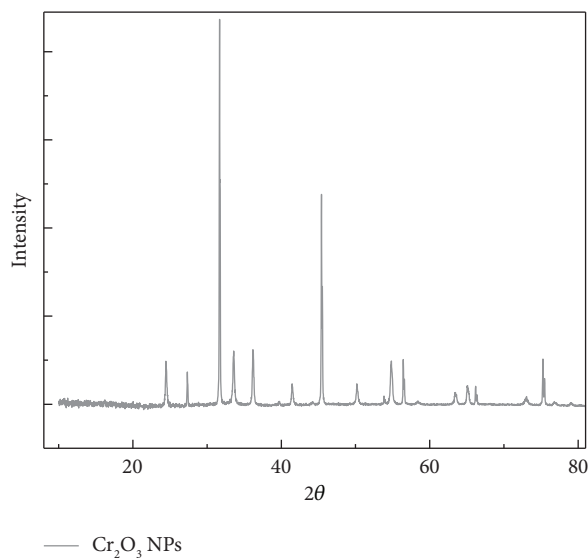
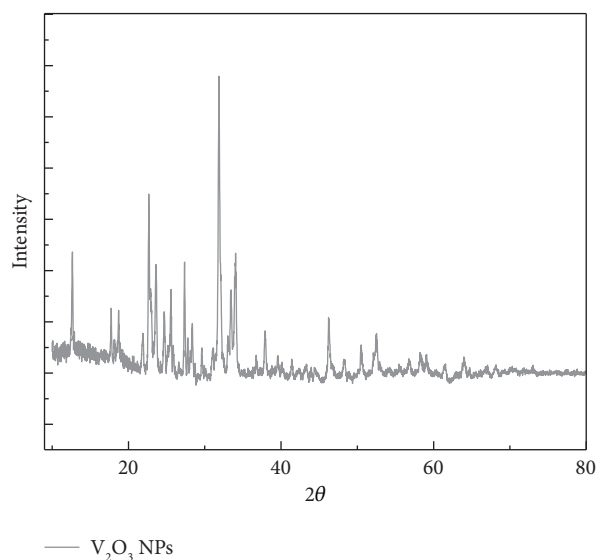
FIGURE 14: XRD pattern of Cr₂O₃ NPs.FIGURE 15: XRD pattern of V₂O₃ NPs.

TABLE 6: X-ray diffraction crystal data for compounds.

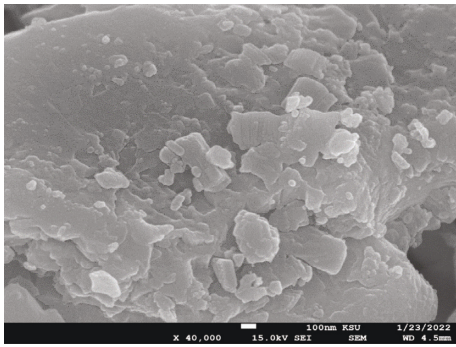
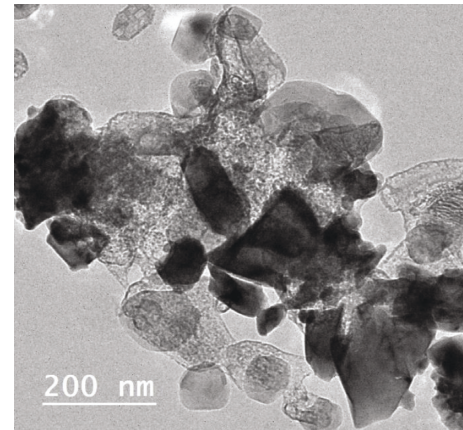
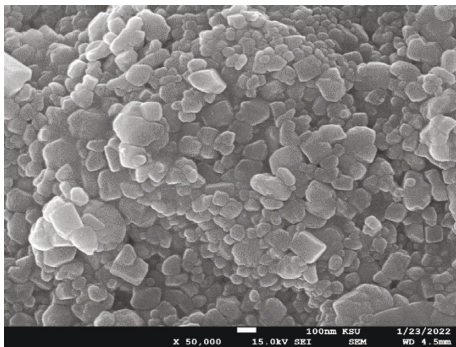
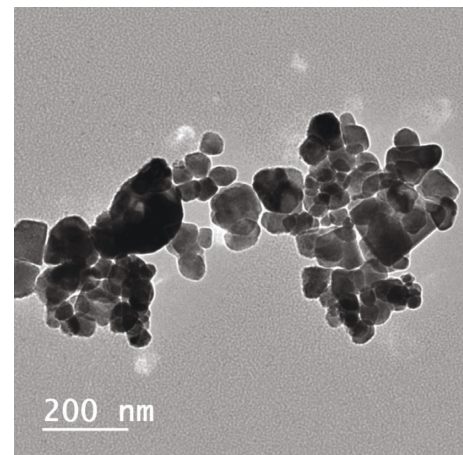
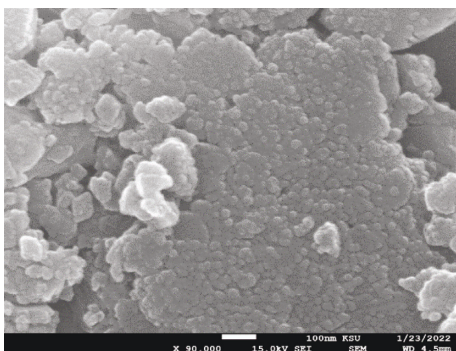
Parameter	Nd (III) complex	Cr (III) complex	V(III) complex
Empirical formula	C ₁₆ H ₁₈ N ₃ NdO ₇	C ₁₄ H ₁₅ N ₃ ClCrO ₅	C ₁₄ H ₁₅ N ₃ ClVO ₅
Formula weight	492.57	392.74	391.68
Crystal system	Cubic	Cubic	Hexagonal
<i>a</i> (Å)	5.6411	5.6408	8.953
<i>b</i> (Å)	5.6411	5.6408	8.953
<i>c</i> (Å)	5.6411	5.6408	8.896
α (°)	90.00	90.00	90.00
β (°)	90.00	90.00	90.00
γ (°)	90.00	90.00	120.00
Volume of unit cell (Å ³)	179.51	179.48	617.5

Metal oxide NPs require connecting with bacterial cells to reach their antibacterial duty. The accepted shapes of contact contain electrostatic attraction [72], van der Waals

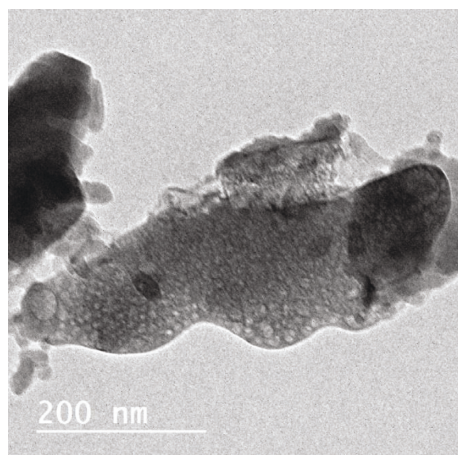
forces [73], receptor-ligand [74], and hydrophobic interactions [75]. MONPs then cross the bacterial membrane and collect along the metabolic pathway, affecting the cell

TABLE 7: X-ray diffraction crystal data of metal oxide nanoparticles.

Parameter	Neodymium oxide	Chromium oxide	Vanadium oxide
Empirical formula	Nd_2O_3	Cr_2O_3	V_2O_5
Formula weight	336.48	151.99	82.94
Crystal system	Hexagonal	Hexagonal	Monoclinic
a (Å)	3.8311	4.9585	10.569
b (Å)	3.8311	4.9585	9.485
c (Å)	6.0004	13.601	5.882
α (°)	90.00	90.00	90.00
β (°)	90.00	90.00	108.419
γ (°)	120.00	120.00	90.00
Volume of unit cell (Å ³)	76.273	289.61	559.5
Particle size (nm)	25.18	55.10	30.43

FIGURE 16: SEM image of Nd_2O_3 NPs.FIGURE 19: TEM image of Nd_2O_3 NPs.FIGURE 17: SEM image of Cr_2O_3 NPs.FIGURE 20: TEM image of Cr_2O_3 NPs.FIGURE 18: SEM image of V_2O_5 NPs.

membrane's shape and function. Afterward, NPs interact with the basic components of bacterial cells, such as DNA, lysosomes, ribosomes, and enzymes, leading to oxidative stress, heterogeneous alterations, changes in cell membrane permeability, electrolyte balance disorders, enzyme inhibition, protein deactivation, and changes in gene expression [76–78]. The most frequently proposed mechanisms are oxidative stress [79–82]. Finally, it may be concluded that Gram-negative bacteria have more antibacterial activity than Gram-positive bacteria due to their membrane shape. There

FIGURE 21: TEM image of V_2O_5 NPs.TABLE 8: Antimicrobial and antioxidant effect (inhibitory zone expressed in $cm \pm SD$).

Compound	Antimicrobial					Antioxidant
	S1	S4	S5	S10	9C	
Nd_2O_3 NPs	1.15 ± 0.21	1.65 ± 0.21	1.15 ± 0.07	1.1 ± 0.14	1.15 ± 0.21	43.5 ± 2.12
Cr_2O_3 NPs	1.1 ± 0.14	1.3 ± 0.14	1.2 ± 0.14	1.15 ± 0.21	1.3 ± 0.14	6.5 ± 0.7
V_2O_5 NPs	0 ± 0.0	2 ± 0.28	1.1 ± 0.0	1.25 ± 0.21	1.5 ± 0.14	51 ± 1.41
Nd(III) complex	1.2 ± 0.14	0 ± 0.0	0 ± 0.0	0 ± 0.0	1.2 ± 0.14	0 ± 0.0
Cr(III) complex	0 ± 0.0	0 ± 0.0	0 ± 0.0	0 ± 0.0	0 ± 0.0	0 ± 0.0

SD: standard deviation.

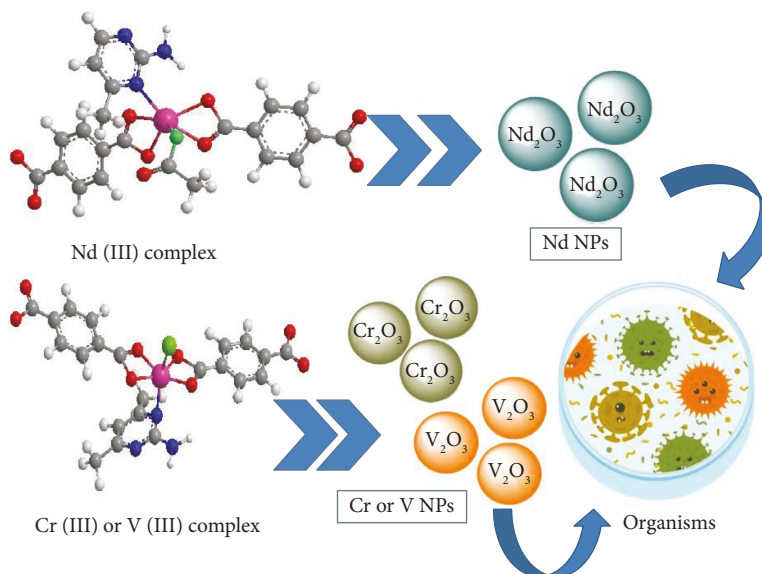


FIGURE 22: The synthesized metal oxide nanoparticles by calcination method and their antimicrobial activity.

are differences in the membrane structure of Gram-positive and Gram-negative bacteria, the most notable of which is the thickness of the peptidoglycan layer. Antibacterial activities of metal oxide NPs are principally attributed to their ability to adhere to bacteria due to their opposite electrical charges, which result in a decrease of the bacterial cell wall. Increased

metal ion concentration on the surface disrupts the cell wall and allows metal ions to seep into the cells. The cell wall or membrane is injured in this method. The current study found that the produced MONPs caused bacterial mortality in Gram-positive and Gram-negative strains. *C. albicans* inhibition zone was largest in V_2O_5 and Cr_2O_3 NPs, respectively.



FIGURE 23: Microbiological activity against *Staphylococcus aureus* ATCC 25923 (1 = Nd_2O_3 , 2 = Cr_2O_3 , and 3 = V_2O_3 nanoparticles).



FIGURE 24: Microbiological activity against *Salmonella typhimurium* ATCC 14028 (1 = Nd_2O_3 , 2 = Cr_2O_3 , and 3 = V_2O_3 nanoparticles).

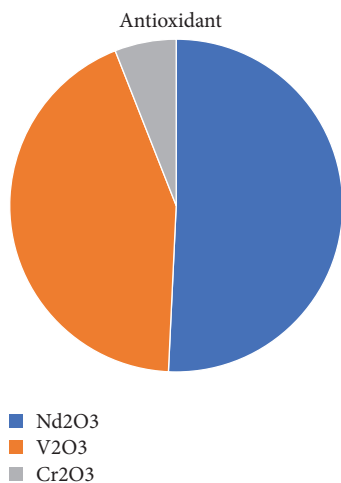


FIGURE 25: Antioxidant effect of MONPs NPs.

4. Conclusion

In this study, platelet Nd_2O_3 , near-spherical Cr_2O_3 , and spherical V_2O_3 NPs were prepared successfully by direct calcination of their mixed ligand complexes. The

characterizations of metal complexes and MONPs revealed their formation of them. All complexes have octahedral geometry. XRD analysis of the complexes and their metal oxides NPs indicated that they have been crystalline and have various crystal systems: cubic for $\text{Nd}(\text{III})$ and $\text{Cr}(\text{III})$ complexes, hexagonal for $\text{V}(\text{III})$ complex, Nd_2O_3 NPs, and Cr_2O_3 NPs, monoclinic for V_2O_3 NPs. According to TEM, the average particle size of MONPs is about 26.9, 53.2, and 21.32 nm for Nd_2O_3 , Cr_2O_3 , and V_2O_3 NPs, respectively, which agree with SEM and XRD results. All compounds showed an excellent antimicrobial effect (except for $\text{Cr}(\text{III})$ complex). MONPs also showed promising results as antioxidants. Overall, calcination was an inexpensive method that can be applied to synthesize other metal oxide NPs to produce better size and morphology with high purity and crystalline. The present study suggests that MONPs have microbiological and antioxidant activity; they can be explored further for biomedical applications.

Data Availability

All data have been included within the article.

Conflicts of Interest

The authors declare that they have no conflicts of interest.

References

- [1] J. Coast, R. D. Smith, and M. R. Millar, "Superbugs: should antimicrobial resistance be included as a cost in economic evaluation?" *Health Economics*, vol. 5, no. 3, 1996.
- [2] R. I. Jaffee and N. E. Promisel, "The science, technology and application of Titanium: proceedings of an international conference organized by the institute of metals, the metallurgical society of aime, and the American society for metals in association with the Japan institute of metals," *Archives of Civil and Mechanical Engineering*, vol. 17, pp. 839–854, 2013.
- [3] L. Madej, "Digital/virtual microstructures in application to metals engineering—a review," *Archives of Civil and Mechanical Engineering*, vol. 17, no. 4, pp. 839–854, 2017.
- [4] A. E. Azab, M. O. Albasha, and A. S. I. Elsayed, "Prevention of nephropathy by some natural sources of antioxidants," *Yangtze Medicine*, vol. 1, no. 4, pp. 235–266, 2017.
- [5] M. Fernández-García, A. Martínez-Arias, J. C. Hanson, and J. A. Rodríguez, "Nanostructured oxides in chemistry: characterization and properties," *Chemical Reviews*, vol. 104, no. 9, pp. 4063–4104, 2004.
- [6] J. A. Rodríguez and M. Fernández-García, *Synthesis, Properties, and Applications of Oxide Nanomaterials*, John Wiley & Sons, New York, NY, USA, 2007.
- [7] J. S. Kim, E. Kuk, K. N. Yu et al., "Antimicrobial effects of silver nanoparticles," *Nanomedicine: Nanotechnology, Biology and Medicine*, vol. 3, no. 1, pp. 95–101, 2007.
- [8] R. J. Aitken, M. Q. Chaudhry, A. B. A. Boxall, and M. Hull, "Manufacture and use of nanomaterials: current status in the UK and global trends," *Occupational Medicine*, vol. 56, no. 5, pp. 300–306, 2006.
- [9] L. Zhang, Y. Jiang, Y. Ding, M. Povey, and D. York, "Investigation into the antibacterial behaviour of suspensions of ZnO nanoparticles (ZnO nanofluids)," *Journal of Nanoparticle Research*, vol. 9, no. 3, pp. 479–489, 2007.

- [10] S.-H. Jung, E. Oh, K.-H. Lee et al., "Sonochemical preparation of shape-selective ZnO nanostructures," *Crystal Growth & Design*, vol. 8, no. 1, pp. 265–269, 2008.
- [11] C. Y. Jimmy, J. Yu, W. Ho, and L. Zhang, "Preparation of highly photocatalytic active nano-sized TiO₂ particles via ultrasonic irradiation," *Chemical Communications*, vol. 19, pp. 1942–1943, 2001.
- [12] J. H. Bang, K. S. Suslick, and K. S. Suslick, "Applications of ultrasound to the synthesis of nanostructured materials," *Advanced Materials*, vol. 22, no. 10, pp. 1039–1059, 2010.
- [13] C.-J. Mao, H.-C. Pan, X.-C. Wu, J.-J. Zhu, and H.-Y. Chen, "Sonochemical route for self-assembled V₂O₅ bundles with spindle-like morphology and their novel application in serum albumin sensing," *The Journal of Physical Chemistry B*, vol. 110, no. 30, pp. 14709–14713, 2006.
- [14] J. Lai, K. V. P. M. Shafi, K. Loos et al., "Doping γ -Fe₂O₃ nanoparticles with Mn(III) suppresses the transition to the α -Fe₂O₃ structure," *Journal of the American Chemical Society*, vol. 125, no. 38, pp. 11470–11471, 2003.
- [15] R. V. Kumar, Y. Kolytyn, X. N. Xu, Y. Yeshurun, A. Gedanken, and I. Felner, "Fabrication of magnetite nanorods by ultrasound irradiation," *Journal of Applied Physics*, vol. 89, no. 11, pp. 6324–6328, 2001.
- [16] D. M. Antonelli and J. Y. Ying, "Synthesis of hexagonally packed mesoporous TiO₂ by a modified sol-gel method," *Angewandte Chemie International Edition in English*, vol. 34, no. 18, pp. 2014–2017, 1995.
- [17] R. Wahab, S. G. Ansari, M. A. Dar, Y. S. Kim, and H. S. Shin, "Synthesis of magnesium oxide nanoparticles by sol-gel process," *Materials Science Forum*, vol. 558–559, pp. 983–986, 2007.
- [18] R. M. Alwan, A. K. Quraish, K. M. Sahan et al., "Synthesis of zinc oxide nanoparticles via sol-gel route and their characterization," *Nanoscience and Nanotechnology*, vol. 5, no. 1, pp. 1–6, 2015.
- [19] M. Farahmandjou and S. Jurablu, "Co-precipitation synthesis of zinc oxide (ZnO) nanoparticles by zinc nitrate precursor," *International Journal of Bio-Inorganic Hybrid Nanomaterials*, vol. 3, no. 179, p. 84, 2014.
- [20] H. Kumar, S. P. Manisha, and P. Sangwan, "Synthesis and characterization of MnO₂ nanoparticles using co-precipitation technique," *International Journal of Chemistry and Chemical Engineering*, vol. 3, no. 3, pp. 155–160, 2013.
- [21] C. Feldmann, H.-O. Jungk, and H. Jungk, "Polyol-mediated preparation of nanoscale oxide particles," *Angewandte Chemie International Edition*, vol. 40, no. 2, pp. 359–362, 2001.
- [22] D. H. Kim, J. W. Kang, T. R. Kim, E. J. Kim, J. S. Im, and J. Kim, "A polyol-mediated synthesis of titania-based nanoparticles and their electrochemical properties," *Journal of Nanoscience and Nanotechnology*, vol. 7, no. 11, pp. 3954–3958, 2007.
- [23] W.-W. Wang, "Microwave-induced polyol-process synthesis of MIIFe₂O₄ (M=Mn, Co) nanoparticles and magnetic property," *Materials Chemistry and Physics*, vol. 108, no. 2–3, pp. 227–231, 2008.
- [24] T. Gnanasekar, S. Valanarasu, I. Loyola Poul Raj et al., "Improved device performance of CuO:Ag photodetectors fabricated by nebulizer spray pyrolysis technique," *Optical Materials*, vol. 124, Article ID 112006, 2022.
- [25] A. Badawi, M. G. Althobaiti, S. S. Alharthi, A. N. Alharbi, A. A. Alkathiri, and S. E. Alomairy, "Effect of zinc doping on the structure and optical properties of iron oxide nanostructured films prepared by spray pyrolysis technique," *Applied Physics A*, vol. 128, no. 2, pp. 1–11, 2022.
- [26] S. Dadashi, R. Poursalehi, and H. Delavari, "Structural and optical properties of pure iron and iron oxide nanoparticles prepared via pulsed Nd:YAG laser ablation in liquid," *Procedia Materials Science*, vol. 11, pp. 722–726, 2015.
- [27] M. A. Gondal, T. A. Saleh, and Q. A. Drmash, "Synthesis of nickel oxide nanoparticles using pulsed laser ablation in liquids and their optical characterization," *Applied Surface Science*, vol. 258, no. 18, pp. 6982–6986, 2012.
- [28] M. Censabella, V. Iacono, A. Scandurra et al., "Low temperature detection of nitric oxide by CuO nanoparticles synthesized by pulsed laser ablation," *Sensors and Actuators B: Chemical*, vol. 358, Article ID 131489, 2022.
- [29] I. P. T. Indrayana, "Nanostructure and optical properties of Fe₃O₄: effect of calcination temperature and dwelling time," *Journal of Physics: Conference Series*, vol. 1341, no. 8, Article ID 82044, 2019.
- [30] M. Gharagozlou, "Synthesis, characterization and influence of calcination temperature on magnetic properties of nano-crystalline spinel co-ferrite prepared by polymeric precursor method," *Journal of Alloys and Compounds*, vol. 486, no. 1–2, pp. 660–665, 2009.
- [31] W. Que, C. H. Kam, Y. Zhou, Y. L. Lam, and Y. C. Chan, "Yellow-to-violet upconversion in neodymium oxide nano-crystal/titania/ormosil composite sol-gel thin films derived at low temperature," *Journal of Applied Physics*, vol. 90, no. 9, pp. 4865–4867, 2001.
- [32] T. L. R. Hewer, E. C. C. Souza, T. S. Martins, E. N. S. Muccillo, and R. S. Freire, "Influence of neodymium ions on photocatalytic activity of TiO₂ synthesized by sol-gel and precipitation methods," *Journal of Molecular Catalysis A: Chemical*, vol. 336, no. 1–2, pp. 58–63, 2011.
- [33] M. S. Lembang, Y. Yulizar, S. Sudirman, and D. O. B. Apriandanu, "A facile method for green synthesis of Nd₂O₃ nanoparticles using aqueous extract of *Terminalia catappa* leaf," *AIP Conference Proceedings*, vol. 2023, pp. 1–7, 2018.
- [34] J.-Z. Xu, J.-J. Zhu, H. Wang, and H.-Y. Chen, "Nano-sized copper oxide modified carbon paste electrodes as an amperometric sensor for amikacin," *Analytical Letters*, vol. 36, no. 13, pp. 2723–2733, 2003.
- [35] J. I. Fasick, N. Lee, and D. D. Oprian, "Spectral tuning in the human blue cone pigment," *Biochemistry*, vol. 38, no. 36, pp. 11593–11596, 1999.
- [36] C. L. Li, H. X. Zhao, T. Takahashi, and M. Matsumura, "Improvement of corrosion resistance of materials coated with a Cr₂O₃/NiCr dilayer using a sealing treatment," *Materials Science and Engineering A*, vol. 308, no. 1–2, pp. 268–276, 2001.
- [37] H. Rotter, M. Landau, M. Carrera, D. Goldfarb, and M. Herskowitz, "High surface area chromia aerogel efficient catalyst and catalyst support for ethylacetate combustion," *Applied Catalysis B: Environmental*, vol. 47, no. 2, pp. 111–126, 2004.
- [38] C. Wu, Y. Xie, and Y. Xie, "Promising vanadium oxide and hydroxide nanostructures: from energy storage to energy saving," *Energy & Environmental Science*, vol. 3, no. 9, pp. 1191–1206, 2010.
- [39] H. J. Song, M. Choi, J.-C. Kim et al., "Li-electroactivity of thermally-reduced V₂O₃ nanoparticles," *Materials Letters*, vol. 180, pp. 243–246, 2016.
- [40] Y. Wang, H. J. Zhang, A. S. Admar et al., "Improved cyclability of lithium-ion battery anode using encapsulated V₂O₃ nanostructures in well-graphitized carbon fiber," *RSC Advances*, vol. 2, no. 13, pp. 5748–5753, 2012.

- [41] H. Li, P. Balaya, and J. Maier, "Li-storage via heterogeneous reaction in selected binary metal fluorides and oxides," *Journal of the Electrochemical Society*, vol. 151, no. 11, Article ID A1878, 2004.
- [42] G. Ma, A. A. M. Aly, and M. S. Al-Fakeh, "Synthesis and characterization of Cu-II, Cd-II and Pb-II coordination polymers derived from 1, 4-benzene and 1, 1'-ferrocenedicarboxylate and 2-aminobenzothiazole," *Journal of the Indian Chemical Society*, vol. 88, pp. 1633–1638, 2011.
- [43] M. S. S. Al-Fakeh, "Synthesis, properties and biological effectiveness of iron oxide nanoparticles via calcinations method," *Oriental Journal of Chemistry*, vol. 36, no. 1, pp. 174–178, 2020.
- [44] M. S. Al-Fakeh, "Synthesis and characterization of nanosized uranyl coordination polymers derived from terephthalic acid and azoles," *Oriental Journal of Chemistry*, vol. 32, no. 2, pp. 1155–1162, 2016.
- [45] A. A. M. Aly, M. Ghandour, and M. S. Alfakeh, "Synthesis and characterization of transition metal coordination polymers derived from 1, 4-benzenedicarboxylate and certain azoles," *Turkish Journal of Chemistry*, vol. 36, no. 1, pp. 69–79, 2012.
- [46] C. Bayrak, "Vibrational spectroscopic studies on the dicyclopropylaminecadmium (II) tetracyanometallate (II) benzene clathrates," *Spectroscopy Letters*, vol. 46, no. 2, pp. 133–140, 2013.
- [47] K. Klai, K. Kaabi, W. Kaminsky, C. Jelsch, F. Lefebvre, and C. Ben Nasr, "A Hirshfeld surface analysis, crystal structure and physicochemical studies of a new Cd(II) complex with the 2-amino-4-methylpyrimidine ligand," *Journal of Molecular Structure*, vol. 1128, pp. 378–384, 2017.
- [48] M. S. Al-Fakeh, R. O. Alsaedi, N. Amiri, and G. A. Allazzam, "Synthesis, characterization, and antimicrobial of MnO and CdO nanoparticles by using a calcination method," *Coatings*, vol. 12, no. 2, p. 215, 2022.
- [49] A. Dbeibia, F. B. Taheur, K. A. Altammar et al., "Control of *Staphylococcus aureus* methicillin resistant isolated from auricular infections using aqueous and methanolic extracts of ephedra alata," *Saudi Journal of Biological Sciences*, vol. 29, no. 2, pp. 1021–1028, 2022.
- [50] A. Mahdhi, N. Leban, I. Chakroun et al., "Extracellular polysaccharide derived from potential probiotic strain with antioxidant and antibacterial activities as a prebiotic agent to control pathogenic bacterial biofilm formation," *Microbial Pathogenesis*, vol. 109, pp. 214–220, 2017.
- [51] E. Biemmi, T. Bein, and N. Stock, "Synthesis and characterization of a new metal organic framework structure with a 2D porous system: (H₂NET₂)₂[Zn₃(BDC)₄]·3DEF," *Solid State Sciences*, vol. 8, no. 3–4, pp. 363–370, 2006.
- [52] K. Nakamoto, "Infrared and raman spectra of inorganic and coordination compounds, part B: applications in coordination, organometallic, and bioinorganic chemistry," *John Wiley & Sons*, vol. 6, 2009.
- [53] S. Ahmad, S. D. Sharma, and M. Isaq, "Vibrational spectral studies of 2-amino-4,6-dimethyl- and 4-amino-2,6-dimethylpyrimidines," *Spectrochimica Acta Part A: Molecular and Biomolecular Spectroscopy*, vol. 52, no. 10, pp. 1369–1373, 1996.
- [54] R. Ramasamy and R. Ranjith, "FT-IR and FT-Raman spectral analysis of 2-amino-4, 6-dimethylpyrimidine," *International Journal of Engineering Research and Applications*, vol. 6, no. 2, pp. 49–54, 2016.
- [55] Y. Kokunov, Y. E. Gorbunova, V. Kovalev, and S. A. Kozyukhin, "Coordination compounds of cobalt (II) and cadmium (II) with 2-amino-4-methylpyrimidine: synthesis, crystal structure, and luminescent properties," *Russian Journal of Inorganic Chemistry*, vol. 58, no. 10, pp. 1187–1192, 2013.
- [56] G. Seguel, B. L. Rivas, and P. Órdenes, "Syntheses and characterizations of copper complexes: interaction of copper acetate dihydrate with 4,4'-bipyridine," *Journal of the Chilean Chemical Society*, vol. 60, no. 3, pp. 3080–3082, 2015.
- [57] M. Sankarganesh, R. Vijay Solomon, and J. Dhavethu Raja, "Platinum complex with pyrimidine- and morpholine-based ligand: synthesis, spectroscopic, DFT, TDDFT, catalytic reduction, in vitro anticancer, antioxidant, antimicrobial, DNA binding and molecular modeling studies," *Journal of Biomolecular Structure and Dynamics*, vol. 39, no. 3, pp. 1055–1067, 2021.
- [58] C. Selvi, D. Nartop, and D. Nartop, "Novel polymer anchored Cr(III) Schiff base complexes: synthesis, characterization and antimicrobial properties," *Spectrochimica Acta Part A: Molecular and Biomolecular Spectroscopy*, vol. 95, pp. 165–171, 2012.
- [59] S. A. Ravichandran, V. P. Rajan, P. V. Aravind, A. Seenivasan, D. G. Prakash, and K. Ramakrishnan, "Characterization of terephthalic acid monomer recycled from post-consumer PET polymer bottles," *Macromolecular Symposia*, vol. 361, no. 1, pp. 30–33, 2016.
- [60] A. A. Hasanein, G. M. El-Subruiti, G. O. Younes, and M. H. Srouf, "Spectral studies on some pyrimidine derivatives in different solvents," *Journal of Solution Chemistry*, vol. 33, no. 12, pp. 1481–1499, 2004.
- [61] M. S. Iorungwa, H. Abuh, R. A. Wuana, P. D. Iorungwa, and N. Surma, "Synthesis, characterization, kinetics, thermodynamics and antimicrobial studies of carbonatotetraamine complexes of Nd(III), Sm(III) and Gd(III) nitrates," *Synthesis (Stuttg)*, vol. 10, no. 100, p. 1, 2020.
- [62] M. S. Refat, T. Altalhi, S. B. Bakare, G. H. Al-Hazmi, and K. Alam, "New Cr(III), Mn(II), Fe(III), Co(II), Ni(II), Zn(II), Cd(II), and Hg(II) gibberellate complexes: synthesis, structure, and inhibitory activity against COVID-19 protease," *Russian Journal of General Chemistry*, vol. 91, no. 5, pp. 890–896, 2021.
- [63] S. Kumar, A. Syed, S. Andotra, R. Kaur Vikas, and S. K. Pandey, "Investigation of synthesized new vanadium (III) complexes of ditolyldithiophosphate ligands by spectroscopic, cyclic voltammetric, DFT, antimicrobial and cytotoxic studies," *Journal of Molecular Structure*, vol. 1154, pp. 165–178, 2018.
- [64] S. A. El-Enein, A. M. Ali, Y. K. Abdel-Monem, M. H. Senna, and M. Madkour, "Novel lanthanide (III) 4-methylbenzoylhydrazide complexes as precursors for lanthanide oxide nanophotocatalysts," *RSC Advances*, vol. 9, no. 72, pp. 42010–42019, 2019.
- [65] P. Jayamurugan, R. Mariappan, K. Premnazeer et al., "Investigation of annealing temperature on structural and morphological properties of Cr₂O₃ nanoparticles for humidity sensor application," *Sens. Imaging*, vol. 18, no. 1, pp. 1–12, 2017.
- [66] A. Kumar, F. Rahman, and A. Khan, "Fabrication and characterization of VO₂ nanoparticles: a simple and low-cost combustion method," *AIP Conference Proceedings*, vol. 2369, no. 1, Article ID 20019, 2021.
- [67] K. Mohanan, N. Subhadrambika, R. S. Selwin Joseyphus, S. S. Swathy, and V. P. Nisha, "Synthesis, spectroscopic characterization, solid state d.c. electrical conductivity and biological studies of some lanthanide(III) chloride complexes

- with a heterocyclic schiff base ligand,” *Journal of Saudi Chemical Society*, vol. 20, no. 4, pp. 379–390, 2016.
- [68] A. A. Gesawat and F. Shakeel, “Synthesis and characterization of ternary complexes of chromium(III) with l-histidine and various diols,” *Arabian Journal of Chemistry*, vol. 10, pp. S2575–S2579, 2017.
- [69] K. Dey, B. B. Bhaumik, and S. Sarkar, “Synthesis and characterization of some vanadium (III) complexes with tetradentate schiff bases,” *Indian Journal of Chemistry*, vol. 43, pp. 773–777, 2004.
- [70] M. Al-fakeh, “Facile direct formation of ZnO nanoparticles from a Zn(II) coordination polymer derived from 5-(3-pyridyl)-1,3,4-oxadiazole-2- thiol and benzimidazole,” *Materials Science: An Indian Journal*, vol. 10, no. 5, pp. 192–198, 2014.
- [71] H. Nagabhushana, R. B. Basavaraj, B. D. Daruka Prasad et al., “Facile EGCG assisted green synthesis of raspberry shaped CdO nanoparticles,” *Journal of Alloys and Compounds*, vol. 669, pp. 232–239, 2016.
- [72] H. Li, Q. Chen, J. Zhao, and K. Urmila, “Enhancing the antimicrobial activity of natural extraction using the synthetic ultrasmall metal nanoparticles,” *Scientific Reports*, vol. 5, no. 1, pp. 11033–11113, 2015.
- [73] I. Armentano, R. A. Carla, F. Elena et al., “The interaction of bacteria with engineered nanostructured polymeric materials: a review,” *The Scientific World Journal*, vol. 2014, no. 6, 18 pages, 2014.
- [74] W. Gao, S. Thamphiwatana, P. Angsantikul, and L. Zhang, “Nanoparticle approaches against bacterial infections,” *Wiley Interdisciplinary Reviews: Nanomedicine and Nanobiotechnology*, vol. 6, no. 6, pp. 532–547, 2014.
- [75] B. Luan, T. Huynh, and R. Zhou, “Complete wetting of graphene by biological lipids,” *Nanoscale*, vol. 8, no. 10, pp. 5750–5754, 2016.
- [76] Y. Xu, M. T. Wei, H. D. Ou-Yang et al., “Exposure to TiO₂ nanoparticles increases *Staphylococcus aureus* infection of HeLa cells,” *Journal of Nanobiotechnology*, vol. 14, no. 1, pp. 34–16, 2016.
- [77] S. Shrivastava, T. Bera, A. Roy, G. Singh, P. Ramachandrarao, and D. Dash, “Characterization of enhanced antibacterial effects of novel silver nanoparticles,” *Nanotechnology*, vol. 18, no. 22, Article ID 225103, 2007.
- [78] W. Yang, C. Shen, Q. Ji et al., “Food storage material silver nanoparticles interfere with DNA replication fidelity and bind with DNA,” *Nanotechnology*, vol. 20, no. 8, Article ID 085102, 2009.
- [79] D. I. Andersson, D. Hughes, and J. Z. Kubicek-Sutherland, “Mechanisms and consequences of bacterial resistance to antimicrobial peptides,” *Drug Resistance Updates*, vol. 26, pp. 43–57, 2016.
- [80] Y. H. Leung, A. M. C. Ng, X. Xu et al., “Mechanisms of antibacterial activity of MgO: non-ROS mediated toxicity of MgO nanoparticles towards *Escherichia coli*,” *Small*, vol. 10, no. 6, pp. 1171–1183, 2014.
- [81] O. Zakharova, A. Y. Godymchuk, A. A. Gusev, S. I. Gulchenko, I. A. Vasyukova, and D. Kuznetsov, “Considerable variation of antibacterial activity of Cu nanoparticles suspensions depending on the storage time, dispersive medium, and particle sizes,” *BioMed Research International*, vol. 2015, Article ID 412530, 11 pages, 2015.
- [82] S. Gurunathan, J. W. Woong Han, A. A. Abdal Daye, V. Eppakayala, and J.-H. Kim, “Oxidative stress-mediated antibacterial activity of graphene oxide and reduced graphene oxide in *Pseudomonas aeruginosa*,” *International Journal of Nanomedicine*, vol. 7, p. 5901, 2012.